Effect of Strain Rate on Microscopic Deformation Behavior of High-density Polyethylene under Uniaxial Stretching.

Takumitsu Kida, Yusuke Hiejima* and Koh-hei Nitta

Department of Chemical and Materials Science, Kanazawa University, Kakuma, Kanazawa 920-1192, Japan

Abstract. The microscopic deformation behaviors such as the load sharing and the molecular orientation of high-density polyethylene under uniaxial stretching at various strain rates were investigated by using *in-situ* Raman spectroscopy. The chains within crystalline phase began to orient toward the stretching direction beyond the yielding region and the orientation behavior was not affected by the strain rate. While the stretching stress along the crystalline chains was also not affected by the strain rate, the peak shifts of the Raman bands at 1130, 1418, 1440 and 1460 cm^{-1}, which are sensitive to the interchain interactions obviously, depended on the strain rate; the higher strain rates lead to the stronger stretching stress or negative pressure on the crystalline and amorphous chains. These effects of the strain rate on the microscopic deformation was associated with the cavitation and the void formation leading to the release of the internal pressure.

1 Introduction

Semi-crystalline polymers such as polyethylene (PE) and polypropylene (PP) have been used in many applications owing to the excellent mechanical properties such as high drawability, toughness, workability, lightweight and so on[1–3]. One of the origins of these mechanical properties is the interminglement of the crystalline and amorphous phase[4–6]. Therefore, the correlations between these complicated morphological and mechanical properties have been widely studied to improve the mechanical properties of semi-crystalline polymers[3,5,7–10].

Although uniaxial stretching is one of the most fundamental deformation process, PE and PP show complicated mechanical response and a long scale structural transformation during deformation[11,12]. In particular, specimens shows inhomogeneous deformation called as the necking in the post-yielding[13,14]. As the specimen is further stretched, necked portion propagates to the entire specimen. During these deformation, microscopic structures transform from the spherulitic structure to the fibrillar structure[5]. It has been established that these structural changes are directly related to the fracture mechanism of semi-crystalline polymers.

For *in-situ* study of the structural changes during deformation, one of the most powerful tools is the rheo-optics, which is the simultaneous measurements of mechanical testing and optical measurements such as birefringence, infrared (IR) spectroscopy, X-ray scattering, or Raman spectroscopy[9,15–28]. Such a technique enables us to detect bulk properties (sress, strain, and strain rate) and coresponding local structural parameters (molecular orientation, microscopic stress, crystallinity, chain conformation) at same time during deformation. Especially, *in-situ* Raman spectroscopy have been useful to evaluate the molecular orientation distribution[22,24] and the microsocpic stress applied to the skeletal chains for PE and PP under deformation[22,25,29].

It has been observed that the mechanical properties of semi-crystalline polymers strongly depend on the strain rates [30–32], though the microscopic origin is unclear at this stage. Although the rheo-Raman spectroscopy was applied, the strain rate effect was not clearly observed [18], presumably due to the low strain rate of ~10^{-3} s^{-1}. Recent development of optical apparatus enable us to measure Raman spectra at sufficiently short exposure time of ~1 s. We have developed custom-made *in-situ* Raman spectroscopy[22,24] with the minimum exposure time during deformation is about 0.1 s. In this study, we performed rheo-Raman spectroscopy of high-density polyethylene (HDPE) to evaluate the effects of strain rate on the microscopic deformation behavior. The molecular orientation and the load sharing of molecular chains of HDPE were evaluated during uniaxial stretching process.

2 Experimental

2.1 Sample preparation

Ziegler-Natta catalyzed HDPE (M_w = 10×10^4, M_w/M_n = 5.9) supplied from TOSOH corporation was used. The

* hiejima@se.kanazawa-u.ac.jp

pellets were melted by a hot press machine for 5 min at 210˚C and 20 MPa followed by quenched in iced water. After the quenching, sample sheets were annealed at 110˚C for 5 h. The volumetric crystallinity was about 66% calculated from the density obtained by Archimedes method, where the crystalline and amorphous density were assumed to be ρ_c = 1000 and ρ_a = 855 kg/m^3, respectively[33]. The notch-shaped specimen (2 mm gauge length and 4 mm width) was used as tensile specimen, which cut out of the sample sheets.

2.2 *In-situ* Raman spectroscopy

To evaluate the real time changes of the microscopic deformation, we developed the *in situ* Raman spectroscopic system by installing a custam made tensile tester to the Raman spectroscopy as shown in Fig.1. The details of *in situ* Raman spectroscopy have been described in the previous papers[22–25]. A DPSS laser (LASOS, Jena, Germany, 639.7 nm in the wavelength, 200 mW in laser power) was used as the incident laser light and a monochromator (PIXIS 100 and Spectra Pro 2300i, Princeton Instruments, Trenton, USA, NJ) was used as the detector. The polarization directions of the incident and scattered light were controlled by a 1/2 wavelength plate and a wire-grid polarizer, respectively. Then, three kinds of polarized Raman spectra (*zz*, *yy*, *zy*) were obtained to evaluate the molecular orientation under uniaxial deformation. In addition, for measuring the changes of the peak position of Raman bands, a 1/4 wavelength plate was used to eliminate the effect of polarization. The laser light was irradiated into the notched portion of the specimen as shonw in Fig.1 (b). Since the two grips of the tensile machine move toward the opposite directions at the same rate, the center of the specimen was irradiated during elongation. The elongation rate was set to 0.5 – 10.0 min^{-1} at 20°C. The *in-situ* Raman spectra were accumulated 10 times with an exposure time of 500 ms.

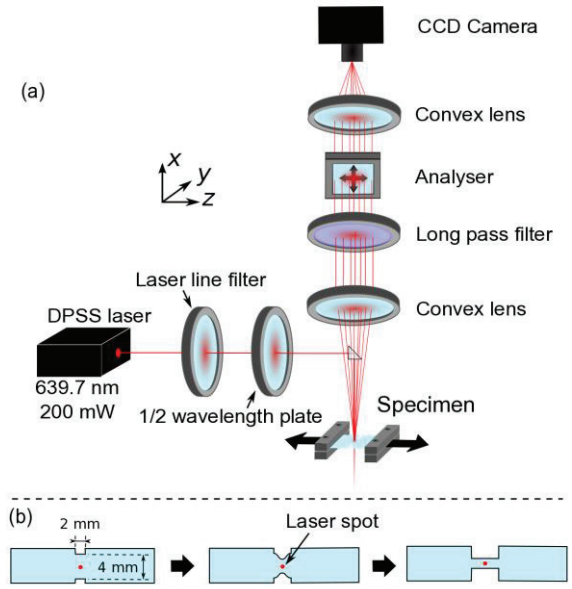

Figure 1. (a) Schematic illustration of *in-situ* Raman spectroscopy system and (b) macroscopic deformatoin behavior of notch-shaped specimen under *in-situ* Raman spectroscopy.

2.2.1 Orientation parameter

The intensity of Raman bands reflects the molecular orientation, which enables us to obtain the orientation parameters[34]. For PE sample, the Raman band at 1130 cm^{-1} assigned to the C-C symmetric stretching mode of crystalline chains has been used to obtain the orientation parameters[22,35]. In this study, two orientation parameters were determined from the intensities of three polarized Raman spectra as follows: [36–39]

$$\langle P_2 \rangle = \frac{3\langle \cos^2\theta \rangle - 1}{2}, \tag{1}$$

$$\langle P_4 \rangle = \frac{35\langle \cos^4\theta \rangle - 30\langle \cos^2\theta \rangle + 3}{8}. \tag{2}$$

Here, θ is the angle between the stretching direction and the principal axis of the Raman tensor. Moreover, the orientation distribution function (ODF) defined as the following equations was determined from the orientation parameters as [38,39]

$$N(\theta) = \sum_{l=0}^{\infty} \left(\frac{2l+1}{2} \right) \langle P_l \rangle P_l(\cos\theta). \tag{3}$$

For the Raman spectroscopy, although only two orientation parameters of $\langle P_2 \rangle$ and $\langle P_4 \rangle$ were obtained, the higher ranks of orientation parameters ($l \geq 6$) can be calculated by maximizing the information entropy. Then, the ODF is written as [24,38,39]

$$N(\theta) = \frac{\exp[\lambda_2 P_2(\cos\theta) + \lambda_4 P_4(\cos\theta)]}{\int_0^{\pi} \sin\theta d\theta \exp[\lambda_2 P_2(\cos\theta) + \lambda_4 P_4(\cos\theta)]}, \tag{4}$$

where λ_2 and λ_4 are the Lagrange multipliers determined to satisfy the following two constraints.

$$\langle P_2 \rangle = \int_0^{\pi} \sin\theta d\theta P_2(\cos\theta) N(\theta), \tag{5}$$

$$\langle P_4 \rangle = \int_0^{\pi} \sin\theta d\theta P_4(\cos\theta) N(\theta). \tag{6}$$

2.2.2 Peak shift

The peak shift $\Delta\nu$ for the Raman bands under uniaxial deformation is defined as the following equation[40,41]:

$$\Delta\nu = \nu - \nu_0, \tag{7}$$

where ν is the peak position at a certain strain and ν_0 is the peak position for the undrawn sample. When the stretching and compression stresses are applied on the molecular chains, the peak shifts have negative and positive values, respectively. The assignments of the Raman bands used in this work is listed in Table 1[42,43]. The anti-symmetric (1063 cm^{-1}) C–C stretching and symmetric (1130 cm^{-1}) C–C stretching vibrational modes correspond to the skeletal chain vibration in the parallel

and perpendicular to the molecular chain axis, respectively. These two Raman bands have been used to evaluate the microscopic stress applied to the skeletal chains of the crystalline phase[22,25]. The Raman bands at 1440 and 1460 cm^{-1} corresponding to the CH_2 bending mode of the amorphous chains, are useful to detect the microscopic pressure on the amorphous phase because CH_2 bending mode is sensitive to the microscopic pressure[25,44]. The Raman band at 1418 cm^{-1} assigned to the CH_2 bending modes of the crystalline chains is also strongly affected by the stress, though the stress sensitivity of 1418 cm^{-1} band is opposite to the other Raman bands; $\Delta\nu_{1418}$ shows positive shifts under stretching stress or negative pressure [44,45].

Table 1. Vibrational and phase assignments for the Raman bands of PE[42,43].

Peak position /cm^{-1}	Vibrational mode*	Phase
1063	ν_{as} (C–C)	Crystalline
1130	ν_{s} (C–C)	Crystalline
1418	δ (CH_2)	Crystalline
1440	δ (CH_2)	Amorphous
1460	δ (CH_2)	Amorphous

* ν_{as}: anti-symmetric stretching, ν_{s}: symmetric stretching
δ: bending

3 Results

3.1 Stress-strain curve

Fig.2 shows the stress-strain curves of HDPE at various strain rates. Before the first yielding point ($\varepsilon \sim 0.4$) corresponding to the maximum stress point, the specimen is deformed homogeneously. Beyond the first yield point, the stress decreases with the strain, and an inhomogeneous deformation called necking initiates around the second yielding point. The yielding stress of these stress-strain curves become higher at higher strain rates. In addition, the shape of stress-strain curve in the yielding region becomes narrower with increasing the strain rates. In the strain-hardening region after yielding, stress gradually increase with increasing the strain at all strain rates.

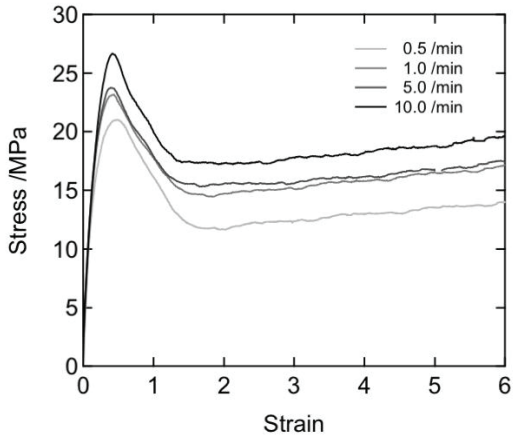

Figure 2. Stress-strain curves elongated at various strain rates.

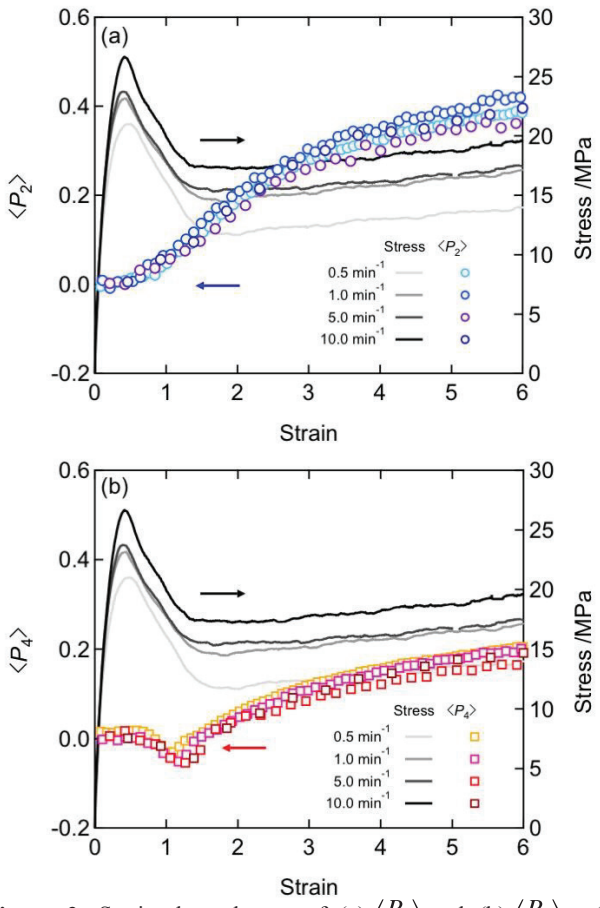

Figure 3. Strain dependences of (a) $\langle P_2 \rangle$ and (b) $\langle P_4 \rangle$ and stress-strain curves elongated at various strain rates.

3.2 Molecular orientation

Fig.3 shows the stress-strain curves and strain dependences of orientation parameters $\langle P_2 \rangle$ and $\langle P_4 \rangle$. In addition, the ODFs at various strain stretched at a strain rate of 0.5 min^{-1} are shonw in Fig.4. The arrows in the figure indicate the vertical axes corresponding to each plot. In the elastic region, the molecular orientation of the crystalline chains remains random since both $\langle P_2 \rangle$ and $\langle P_4 \rangle$ were almost zero and ODF was constant irrespective of the polar angle. After the first yielding point, $\langle P_2 \rangle$ began to increase with increasing the strain, indicating that the crystalline chains begin to orient toward the stretching direction. On the contrary, $\langle P_4 \rangle$ decreased after the first yield point and the ODF showed a broad peak at an intermediate direction (30-50˚). Very similar results have been reported by *in-situ* WAXD[9,46] and Raman spectroscopy of HDPE[22,23] and iPP[24]. This oblique orientation in the yielding region is explained by the plastic deformation such as the intracrystalline slip[9,46] or the fragmentatioin process into the lamellar cluster units[22]. In the strain-hardening region, both orientation parameters drastically increased with the strain, and reached asymptotic values in the highly-strained region ($\varepsilon > 4$). The ODFs showed sharp peak at $\theta = 0$, suggesting that the molecular chains within the crystalline phase simply orient in the stretching direction. These molecular orientation behavior of the crystalline chains is unchanged with the strain rates, indicating that

the microscopic structural transformation are little affected by the strain rate, though the macroscopic stress-strain behavior is obviously affected.

3.3 Load sharing

Fig.5 shows the strain dependences of the peak shifts for the crystalline chains. In the elastic region, it was found that almost no stress is applied to the crystalline chains because peak shifts of crystalline chains remain zero. These results indicate that in the elastic region the stress mainly concentrates on the amorphous chains, which is in good agreement with the previous data of SAXS measurements [26,27] and the microscopic observation [47]. $\Delta\nu_{1063}$ drastically decreased in the yielding region followed by a weak red shifts, indicating that the stretching stress is applied to the crystalline chains beyond the first yielding region. $\Delta\nu_{1130}$ increased beyond the first yield point and showed a maximum around the second yield point, where $\Delta\nu_{1418}$ showed a minimum. These results indicate that the compression stress is applied to the intermolecular direction of the crystalline chains [25,44,45] due to the densification caused by the necking. Beyond the yielding region, $\Delta\nu_{1130}$ rapidly decreased with strain, approaching an asymptotic value in the highly-strained region, suggesting that the stretching stress is applied to the crystalline chains. The sharp increase of $\Delta\nu_{1418}$ is explained by the expansion of the orthorhombic crystalline structure due to the stretching stress [25,45]. While the peak shifts depended little on the strain rate up to the yielding region, $\Delta\nu_{1130}$ and $\Delta\nu_{1418}$ in the strain-hardening region appreciably depended on the strain rate. Because these two bands reflect the microscopic structural transformation perpendicular to the molecular chain, the strain rate dependence of the peak shifts is explained by the microscopic deformation in the perpendicular to the molecular chain axis. It is noteworthy that the strain rate dependence of the $\Delta\nu_{1063}$ corresponding to the stress along the molecular chain axis is negligible during the entire strain range.

Fig.6 shows the strain dependences of the peak shifts for the amorphous CH_2 bending modes. In the elastic region, both peak shifts $\Delta\nu_{1440}$ and $\Delta\nu_{1460}$ were almost zero, suggesting that no microscopic pressure is applied to the amorphous phase. After the first yield point, $\Delta\nu_{1440}$ and $\Delta\nu_{1460}$ began to increase and show maximum points around the second yielding points. The maximum values around the second yielding point of $\Delta\nu_{1440}$ and $\Delta\nu_{1460}$ were obviously larger than those of the crystalline phase ($\Delta\nu_{1130}$ and $\Delta\nu_{1418}$), indicating that the compression stress under necking is more concentrated on the amorphous phase than in the crystalline chains. Beyond the yielding region, stretching stress applied initially to the amorphous phase because both peak shifts of amorphous chains showed a decrease with the strain. In the highly-strained region, the microscopic load sharing of the amorphous phase remained essentially constant, suggesting that the microscopic structural transformation has been practically completed in the yielding region.

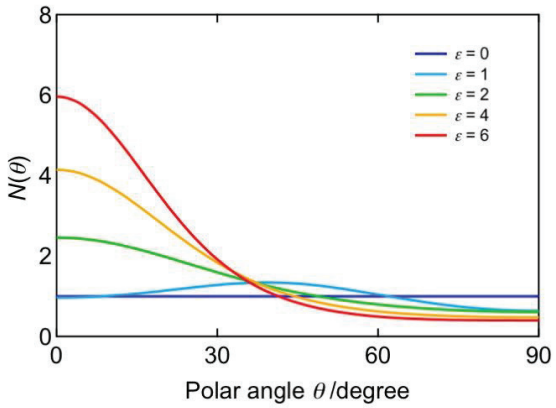

Figure 4. ODFs at various strains during elongation at various strain rates.

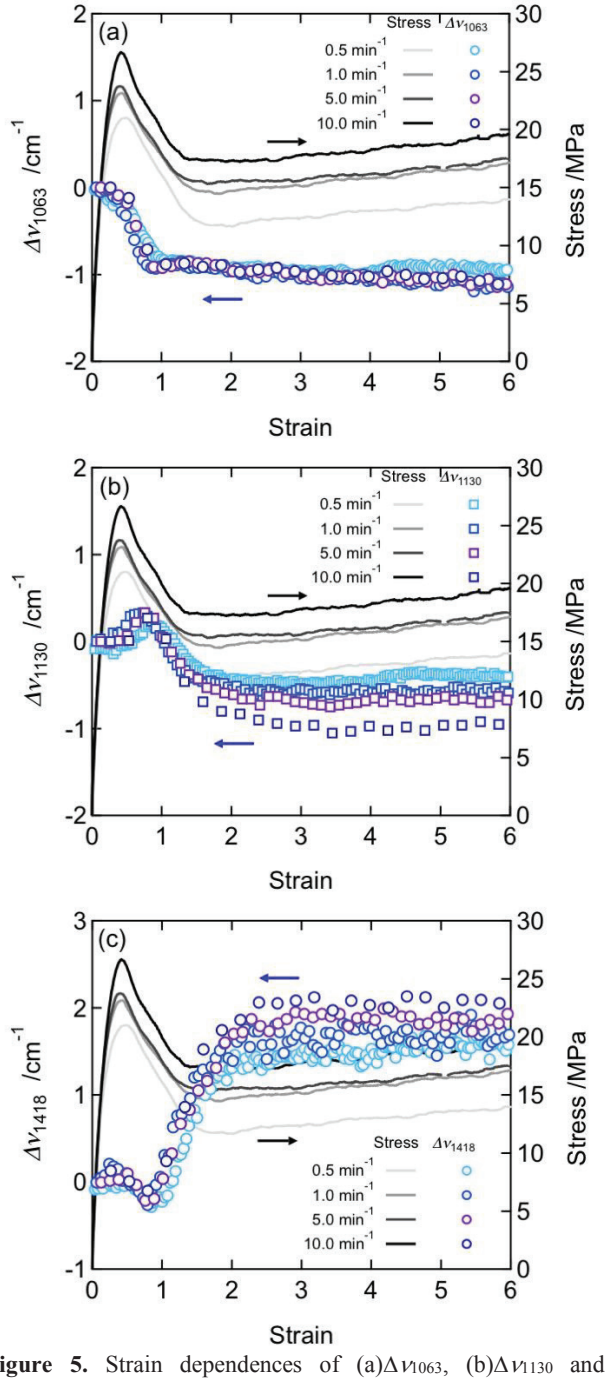

Figure 5. Strain dependences of (a)$\Delta\nu_{1063}$, (b)$\Delta\nu_{1130}$ and (c)$\Delta\nu_{1418}$ along with stress-strain curves elongated at various strain rates.

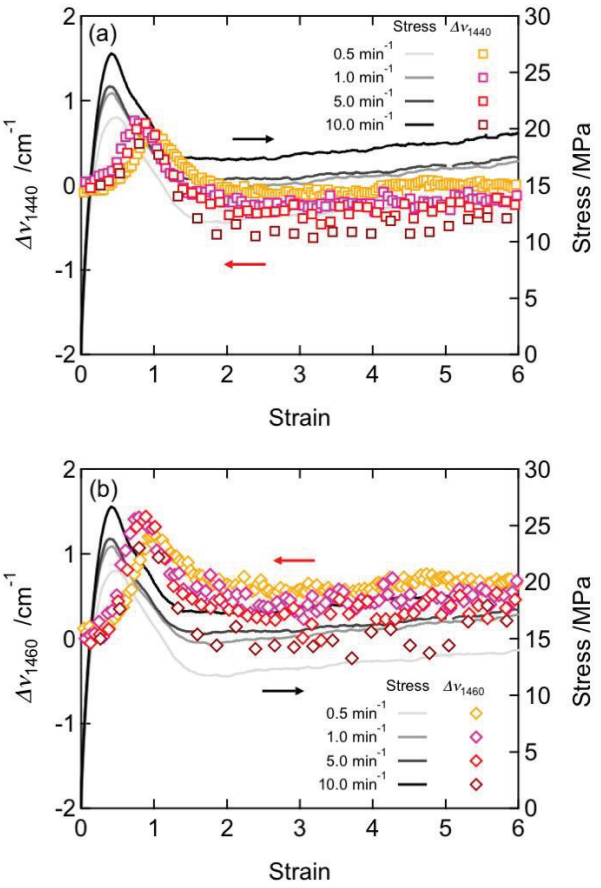

Figure 6. Strain dependences of (a)$\Delta\nu_{1440}$ and (b)$\Delta\nu_{1460}$ along with stress-strain curves elongated at various strain rates.

The strain rate dependences of $\Delta\nu_{1440}$ and $\Delta\nu_{1460}$ were observed in the strain-hardening region, as observed for the crystalline bands at 1130 and 1418 cm^{-1}. Then, it is suggestd that a higher strain rate leads to a stronger stretching loading on the amorphous chains.

4 Discussion

While the molecular orientation are independent of strain rate, the peak shifts of the Raman bands except for the 1063 cm^{-1} band obviously depend on strain rate. This is because they are sensitive to the microscopic deformation in the perpendicular to the molecular chain axis. Then, while the overall microscopic deformation remains essentially the same, the strain rate is likely to affect the interchain interactions.

It has been proposed that the increase of the strain rate promotes the cavitation and the void formation with necking[10,32], resulting in the release of the internal negative pressure which is induced by the Poisson contraction during the uniaxial stretching[48,49]. Under hydrostatic pressure [44], the CH_2 bending modes at 1440 and 1460 cm^{-1} and the C–C symmetric stretching mode at 1130 cm^{-1} show blue shifts and the CH_2 bending modes at 1418 cm^{-1} shows red shift. Then, the large shift beyond the yielding region (red shift for the 1130, 1440 and 1460 cm^{-1} and blue shift for the 1418 cm^{-1}) can be considered to result from the formation of cavitation and voids. The data of the load sharing and the molecular orientation of the amorphous chains were indispensable to reveal the effect of strain rate on the microscopic deformation mechanism.

5 Conclusions

In-situ Raman spectroscopy was performed to investigate the microscopic deformation during uniaxial stretching and to clarify the effects of the strain rate. Beyond the yielding region, the crystalline chains were stretched and compressed along and perpendicular to the molecular chain axis, respectively. In addition, the compression stress was found to be also applied to the amorphous phase due to the inhomogeneous deformation of the specimen under necking. Moreover, the crystalline chains oriented in the intermediate direction accompanied with the plastic deformation of the crystalline phase. In the strain-hardening region, the crystalline chains simply oriented in the stretching direction, and the stretching stress was applied to both crystalline and amorphous chains. Although the overall deformation mechanism of the microscopic structure was independent of the strain rates, interchain interactions of the crystalline and amorphous chains were affected by the strain rate. These effects of strain rate were caused by the formation of cavitation and voids during the yielding.

References

[1] I.M. Ward, J. Sweeney, *Mechanical Properties of Solid Polymers: 3rd edition* (Wiley&Sons, London, 2013)

[2] I.M. Ward, *Structure and properties of oriented polymers* (Chapman&Hall, London, 1997)

[3] G. Strobl, *The Physics of Polymers, 2nd ed.* (Springer, Verlag Berlin Heidelberg, 1996)

[4] R. Seguela, J. Polym. Sci. Part B Polym. Phys. **43**, 1729 (2005)

[5] A. Peterlin, J. Mater. Sci. **6**, 490 (1971)

[6] E.F. Oleinik, Polym. Sci. Ser. C. **45**, 17 (2003)

[7] K.-H. Nitta, M. Takayanagi, J. Macromol. Sci. Part B Phys. **42**, 107 (2003)

[8] K.-H. Nitta, M. Takayanagi, J. Polym. Sci. Part B Polym. Phys. **37**, 357 (1999)

[9] Z. Jiang, Y. Tang, J. Rieger, H.-F. Enderle, D. Lilge, S. V. Roth, R. Gehrke, Z. Wu, Z. Li, Y. Men, Polymer **50**, 4101 (2009)

[10] M. Kuriyagawa, K.-H. Nitta, Polymer **52**, 3469 (2011)

[11] K.-H. Nitta, T. Ishiburo, J. Polym. Sci. Part B Polym. Phys. **40**, 2018 (2002)

[12] K. Hong, A. Rastogi, G. Strobl, Macromolecules **37**, 10165 (2004)

[13] P.I. Vincent, Polymer **1**, 7 (1960)

[14] C. G'sell, N. Aly-Helal, J. Jonas, J. Mater. Sci. **18**, 1731 (1983)

[15] M. Plass, R. Streck, J. Nieto, H.W. Siesler, Macromol. Symp. **265**, 166 (2008)

[16] H.W. Siesler, Polym. Bull. **12**, 481 (1984)

[17] S. Onogi, A. Tanaka, Y. Ishikawa, T. Igarashi, Polym. J. **7**, 467 (1975)

[18] P. Tarantili, A. Andreopoulos, C. Galiotis, Macromolecules **31**, 6964 (1998)

[19] H. Shinzawa, W. Kanematsu, I. Noda, Vib. Spectrosc. **70**, 53 (2014)

[20] M. Mizushima, T. Kawamura, K. Takahashi, K.-H. Nitta, Polym. Test. **38**, 81 (2014)

[20] M. Mizushima, T. Kawamura, K. Takahashi, K.-H. Nitta, Polym. Test. **38**, 81 (2014)

[21] Y. Tang, Z. Jiang, Y. Men, L. An, H.F. Enderle, D. Lilge, S. V. Roth, R. Gehrke, J. Rieger, Polymer **48**, 5125 (2007)

[22] T. Kida, T. Oku, Y. Hiejima, K.-H. Nitta, Polymer **58**, 88 (2015)

[23] T. Kida, Y. Hiejima, K.-H. Nitta, Polym. Test. **44**, 30 (2015)

[24] T. Kida, Y. Hiejima, K.-H. Nitta, Express Polym. Lett. **10**, 701 (2016)

[25] T. Kida, Y. Hiejima, K.-H. Nitta, Int. J. Exp. Spectrosc. Tech. **1**, 1 (2016)

[26] B. Xiong, O. Lame, J.-M. Chenal, C. Rochas, R. Seguela, G. Vigier, Polymer **55**, 1223 (2014)

[27] B. Xiong, O. Lame, J.-M. Chenal, C. Rochas, R. Seguela, G. Vigier, Macromolecules **48**, 2149 (2015)

[28] B. Xiong, O. Lame, J.-M. Chenal, C. Rochas, R. Seguela, Express Polym. Lett. **10**, 311 (2016)

[29] J.C. Rodríguez-Cabello, J.C. Merino, T. Jawhari, J.M. Pastor, J. Raman Spectrosc. **27**, 463 (1996)

[30] S. Hobeika, Y. Men, G. Strobl, Macromolecules **33**, 1827 (2000)

[31] T. Liu, I.R. Harrison, Polymer **29**, 233 (1988)

[32] P.-Y. Ben Jar, Polym. Eng. Sci. **54**, 1871 (2014)

[33] J. Brandrup, E. Immergut, E.A. Grulke, *Polymer Handbook* (Wiley&Sons, New York, 1990)

[34] M. Tanaka, R.J. Young, J. Mater. Sci. **41**, 963 (2006)

[35] M. Pigeon, R.E. Prud'homme, M. Pezolet, Macromolecules **24**, 5687 (1991)

[36] S. Frisk, R.M. Ikeda, D.B. Chase, J.F. Rabolt, Appl. Spectrosc. **58**, 279 (2004)

[37] M. Richard-Lacroix, C. Pellerin, Macromolecules **46**, 5561 (2013)

[38] D.I. Bower, J. Polym. Sci. Polym. Phys. Ed. **10**, 2135 (1972)

[39] D.I. Bower, J. Polym. Sci. Polym. Phys. Ed. **19**, 93 (1981)

[40] R.P. Wool, Polym. Eng. Sci. **20**, 805 (1980)

[41] R.P. Wool, R.S. Bretzlaff, B.Y. Li, C.H. Wang, R.H. Boyd, J. Polym. Sci. Part B Polym. Phys. **24**, 1039 (1986)

[42] M. Gall, P. Hendra, C. Peacock, Polymer **13**, 104 (1972)

[43] M. Gall, P. Hendra, O. Peacock, M.E.A. Cudby, H.A. Willis, Spectrochim. Acta Part A Mol. Spectrosc. **28A**, 1485 (1972)

[44] Y. Zhao, J. Wang, Q. Cui, Z. Liu, M. Yang, J. Shen, Polymer **31**, 1425 (1990)

[45] J. Otegui, J.F. Vega, S. Martin, V. Cruz, A. Flores, C. Domingo, J. Martinez-Salazar, J. Mater. Sci. **42**, 1046 (2007)

[46] R. Hiss, S. Hobeika, C. Lynn, G. Strobl, Macromolecules **32**, 4390 (1999)

[47] K.-H. Nitta, M. Takayanagi, J. Mater. Sci. **38**, 4889 (2003)

[48] B. Xiong, O. Lame, J.M. Chenal, C. Rochas, R. Seguela, G. Vigier, Polymer **54**, 5408 (2013)

[49] C. Fond, J. Polym. Sci. Part B Polym. Phys. **39**, 2081 (2001)